HHS Public Access

Author manuscript

Nat Immunol. Author manuscript; available in PMC 2018 August 23.

Published in final edited form as:

Nat Immunol. 2018 March ; 19(3): 255–266. doi:10.1038/s41590-018-0052-z.

Toll-like receptor 9 antagonizes antibody affinity maturation

Munir Akkaya[1], **Billur Akkaya**[2], **Ann S. Kim**[1], **Pietro Miozzo**[1], **Haewon Sohn**[1], **Mirna Pena**[1], **Alexander S. Roesler**[1], **Brandon P. Theall**[1], **Travis Henke**[1], **Juraj Kabat**[3], **Jinghua Lu**[1], **David W. Dorward**[4], **Eric Dahlstrom**[4], **Jeff Skinner**[1], **Louis H. Miller**[5], and **Susan K. Pierce**[1]

[1]Laboratory of Immunogenetics, National Institute of Allergy and Infectious Diseases, National Institutes of Health, Rockville, Maryland [2]Laboratory of Immunology, National Institute of Allergy and Infectious Diseases, National Institutes of Health, Bethesda, MD [3]Research Technologies Branch, National Institute of Allergy and Infectious Diseases, National Institutes of Health, Bethesda, MD [4]Research Technologies Branch, National Institute of Allergy and Infectious Diseases, National Institutes of Health, Hamilton, MT [5]Laboratory of Malaria and Vector Research, National Institute of Allergy and Infectious Diseases, National Institutes of Health, Rockville, Maryland

Abstract

Key events in T cell-dependent antibody responses, including affinity maturation, are dependent on the B cell's presentation of antigen to helper T cells at critical check points in germinal center formation in secondary lymphoid organs. Here we show that Toll-like receptor 9 (TLR9) signaling blocked the ability of antigen-specific B cells to capture, process and present antigen and to activate antigen-specific helper T cells *in vitro*. In a mouse model *in vivo* and in a human clinical trial the TLR9 agonist, CpG, enhanced the magnitude of the antibody response to a protein vaccine but failed to promote affinity maturation. Thus, TLR9 signaling may enhance antibody titers at the expense of the ability of B cells to engage in germinal center events that are highly dependent on B cells' antigen capture and presentation.

INTRODUCTION

Key checkpoints in T cell-dependent antibody responses *in vivo* are dependent on antigen-specific B cell-T cell interactions. The initiation of T cell-dependent antibody responses occurs in secondary lymphoid organs and is dependent on the stable interaction of antigen-primed helper T (T_H) cells with activated antigen-specific B cells through peptide-major histocompatibility complex (MHC) class II presented on the B cell surface [reviewed in [1, 2, 3, 4]]. Depending, in part, on the quality of the B cell-T_H cell interaction, B cells either

Correspondence should be addressed to S.K.P. (spierce@nih.gov).

AUTHOR CONTRIBUTIONS

M.A. and S.K.P. conceived the project and designed the experiments. S.K.P secured the funding. M.A., B.A., A.S.K., P.M., H.S., M.P., A.S.R., B.P.T, J.L., T.H. carried out the experiments. M.A., B.A., A.S.K., P.M., H.S., J.K., D.W.D., J.S., J.L., E.D., L.H.M., S.K.P. analyzed the data. M.A., S.K.P. wrote the manuscript.

enter germinal centers (GCs) or differentiate into short-lived plasma cells (PCs) and GC-independent memory B cells (MBCs) [2]. Within GCs, the competitive process of affinity selection occurs based on the ability of B cell receptors (BCRs) to capture, process and present antigen to T follicular helper (T_{FH}) cells. The B cells' successful presentation of antigen to T_{FH} cells ultimately results in the differentiation of GC B cells to long-lived MBCs and PCs.

B cells also express germline encoded Toll-like receptors (TLRs) that respond to microbial products expressing pathogen-associated molecular patterns [5, 6, 7]. The dual expression of the BCR and TLRs allows B cells to modulate the outcome of antigen encounter in the presence of pathogens (reviewed in [5, 6]). Indeed, TLR9 signaling has been shown to enhance the response of B cells to antigens coupled to the TLR9 agonist CpG in terms of proliferation and differentiation to antibody secreting cells both *in vitro* and *in vivo*. In addition to signaling for B cell activation, the BCR functions to transport bound antigen to specialized intracellular compartments in which the antigen is degraded and the resulting peptides are bound to MHC class II molecules that are presented on the cell surface for recognition by antigen-specific T_H cells [8]. At present, we do not know whether TLR signaling influences the antigen processing and presentation function of the BCR.

Although TLR signaling has the potential to amplify humoral responses to antigen[9, 10], B-cell intrinsic TLR signaling does not appear to be required for adjuvant-enhanced T cell-dependent antigen-specific antibody responses *in vivo* [11]. Although adjuvants can influence several qualities of antibody responses including kinetics, magnitude and breadth [12], until recently the ability of adjuvants to augment B cell GC responses including somatic hypermutation (SHM) events has not been explored. Recently, the HIV envelope (Env)-specific B cell receptor response in nonhuman primates to immunization with Env formulated with eight different adjuvants, including ones that target TLR pathways, were compared[13]. The adjuvants increased Env-specific antibody titers, but remarkably, did not increase SHM frequencies essential for the development of broadly neutralizing antibodies in this system.

Here we provide evidence that although TLR9 signaling enhanced BCR-induced B cell proliferation and differentiation to antibody-secreting cells, TLR9 signaling reduced the ability of B cells to capture, process and present antigen, and to interact with and to activate antigen- specific T_H cells *in vitro* which was detrimental to the establishment of high-affinity, long-lived Ab responses *in vivo*.

RESULTS

The impact of TLR9 signaling on BCR-dependent B cell activation

We determined the effect of CpG on several antigen-driven BCR-signaling functions in mouse splenic B cells purified by negative selection and treated with soluble polyclonal $F(ab)'_2$ IgM-specific antibody (Anti-IgM), CpG or Anti-IgM plus CpG. These included: phosphorylation of kinases in the BCR signaling pathway (Fig. 1a–d, Fig. S1a–c); Ca^{2+} responses (Fig. 1e, Fig. S1d); the mRNA expression for cytokines at 3h post stimulation (Fig. 1f) and cytokine protein levels at 18h (Fig. 1g); the proliferative responses of B cells

(Fig. 1h); and IgM (Fig. 1i) and IgG (Fig. 1j) secretion in culture supernatants over seven days. We determined that although Anti-IgM or CpG treatment resulted in different patterns of kinase phosphorylation, the result of treatment with both Anti-IgM and CpG was additive, Anti-IgM concentration dependent and for CpG responses, dependent on TLR9 expression (Fig. 1a–c, Fig. S1a–c). In contrast, B cells only fluxed Ca^{2+} in response to Anti-IgM (Fig. 1e, Fig. S1d) and this response was unaffected by CpG. CpG and Anti-IgM synergized to induce high expression of IL-2 and TNF at both mRNA and protein levels whereas the CpG-induced expression of IL-6 and IL-10 was substantially antagonized by Anti-IgM (Fig. 1f,g). CpG enhanced the proliferation of sub-optimal Anti-IgM treated B cells in a TLR9-dependent fashion (Fig. 1h, Fig. S1e,f). CpG induced IgM secretion by B cells that was weakly antagonized by Anti-IgM (Fig. 1i), whereas Anti-IgM enhanced the CpG-induced secretion of IgG by IgG^{+}-depleted B cells (Fig. 1j, Fig. S1g). Taken together, these results demonstrate the ability of CpG to alter the B cells response to BCR crosslinking and *vice versa.*

We also measured by qPCR the transcription of three factors which influence the PC fate of B cells[14]. CpG alone and CpG plus Anti-IgM decreased the expression of *Bcl6* (encoding a key transcriptional repressor for PC differentiation) the expression of which is critical for maintenance of B cell GC reactions (Fig. 1k) but increased the expression of *Prdm1* (encoding BLIMP-1, a transcription factor promoting PC differentiation) (Fig. 1i) and *Aicda* (encoding AID which is upregulated when B cells differentiate toward PCs) (Fig. 1m). Taken together, these results provide evidence that TLR9 signaling has the potential to drive B cells toward PC differentiation and away from GC responses.

BCR internalization and trafficking of soluble antigen

We measured the ability of the BCRs to internalize soluble antigen, either Anti-IgM by C57BL/6 B cells or hen egg lysozyme (HEL) by HEL-specific B cells from MD4 transgenic mice, in the presence or absence of CpG. CpG did not affect the rate or magnitude of BCR internalization in either case (Fig. S2a,b). We characterized the intracellular vesicles into which Anti-IgM was internalized by incubating B cells with Anti-IgM-coated electron-dense metal particles and imaging the cells by transmission electron microscopy and tomography. Quantification of three dimensional reconstructions of the images showed Anti-IgM-particles in morphologically similar compartments in both CpG-treated and untreated cells (Fig. S2c–g).

Once internalized into early endosomes, the BCR traffics antigen to increasingly acidic late endosomes. We measured the fluorescence intensity (FI) of HEL-specific MD4 B cells internalizing soluble HEL conjugated to the pH sensitive dye, pHrodo, the FI of which increases with decreases in pH. For both CpG-treated and untreated B cells, the FI increased at the same rate for the first 20 min at 37 °C (Fig. 2a,b, Fig. S3a). In the absence of CpG, the FI of the B cells continued to increase with time. In contrast, the FI of the CpG-treated B cells increased little after 30 min and the block in trafficking was TLR9 dependent (Fig. 2a,b).

We further characterized the endosomal compartments into which the BCR internalized rhodamine-conjugated HEL in the presence or absence of CpG by confocal microscopy (Fig.

2c–e). Cells were fixed, stained with DAPI to label nuclei, and antibodies specific for either: CD71, the transferrin receptor, a marker of early endosomes, LAMP1, a marker of late endosomes, or H2M, a MHC class II chaperon present in antigen-processing compartments. Three dimensional colocalizations of HEL with CD71, LAMP1 or H2M were quantified by Imaris (Fig. 2c–e, Fig. S3b,c). HEL colocalized with CD71 in early endosomes at 10 min and CpG treatment had no significant effect on colocalization (Fig. 2c). Colocalization of HEL with both LAMP1 and H2M increased from 10 min (Fig. S3b,c) to 60 min and treatment with CpG significantly diminished the 60 min colocalization (Fig. 2d,e). Taken together, these data indicate that TLR9 signaling compromised the BCR's delivery of antigen into late endosomes and the antigen processing compartments.

TLR9 signaling affects B cell responses to membrane-bound antigen

We determined the effect of CpG treatment on B cell responses to antigen incorporated into fluid planar lipid bilayers. MD4 HEL-specific B cells were labeled using a Dylight 649-Fab Anti-IgM and placed on bilayer contained Alexa Fluor 488-labeled HEL and live cell imaging was carried out by total internal reflection fluorescence (TIRF) microscopy [15, 16, 17] (Fig. 3a and supplementary videos S1a–S1c). When pretreated for 20 min with CpG, the B cells spread more robustly over the HEL-containing bilayer, covering larger areas as compared to untreated B cells (Fig. 3a,b) but did not form a well-organized central synapse and accumulated less BCR (Fig. 3c) and HEL (Fig. 3d) in the contact area. B cells pretreated for 60 min with CpG behaved similarly but contracted after 90s and accumulated less BCR but comparable amounts of HEL as compared to the untreated B cells (Fig. 3d) suggesting an antigen-independent component of BCR accumulation as described earlier[18]

We also measured the BCR-dependent internalization of HEL incorporated into plasma membrane sheets (PMS) by HEL-specific MD4 B cells. B cells were labeled with Dylight 649-Fab Anti-IgM and placed for 30 min at 37 °C on CM-DiI- labeled PMS into which Alexa Fluor 488-HEL was incorporated. Confocal *z*-stack images were obtained and reconstituted as an *x* and *z* view (Fig. 3e) using Matlab programs to quantify only the internalized antigen, excluding antigen tethered on the PMS surface (Fig. 3f). In the absence of CpG, B cells internalized HEL from the PMS, but in the presence of CpG, HEL internalization was markedly less, as measured by either the percent of the HEL in the bilayer that was internalized or the total HEL internalized (Fig. 3f). We also determined the degree of colocalization of the BCR and HEL, and of HEL and fragments of the PMS in 3D-reconstructed images of the confocal *z*-stacks of B cells placed on HEL-containing PMS for 30 min (Fig. 3g and Supplementary videos 2a,b). HEL, BCR and fragments of the PMS above the contact area with the PMS surface indicate internalization (Fig. 3g). In the absence of CpG, B cells were frequently observed in contact areas in which the PMS had been cleared in contrast to CpG-treated B cells that were observed in areas covered by the PMS. Videos of 3D surface images showed that in both CpG-treated and untreated cells little antigen was retained on the B cell surface. In the *xy* and *xz* cross sections of B cells not treated with CpG, the BCR and HEL and PMS fragments to which HEL was bound are evidently inside the cell (Supplementary videos 2a,b) where the BCR and HEL colocalized (Fig. 3h) as did HEL and PMS fragments (Fig. 3i). However, for CpG-treated B cells although BCR and HEL were present intracellularly, very few PMS fragments were evident

(Fig. 3g). Co-localization of HEL and the BCR were similar to untreated cells (Fig. 3h), however, the co-localization of HEL and fragments of the PMS were significantly decreased (Fig. 3i). The lack of PMS in CpG-treated B cells suggests that antigen taken up by BCRs in the presence of CpG did not involve pulling the antigen and attached PMS into the cell but likely was the result of the internalization of antigen that was not tightly attached to the PMS.

Gene transcription and the expression of B cell surface markers

An RNA seq analysis was carried out on untreated B cells and B cells treated with Anti-IgM or CpG alone or together for 4 h. A venn diagram (Fig. 4a) and a principle component analysis (Fig. 4b) of the results showed a remarkable separation of the transcription profiles of B cells under the different stimulation conditions. Thus, treatment of B cells with Anti-IgM and/or CpG resulted in activation of a distinct transcriptional program. An Ingenuity Pathway Analysis of the differentially expressed genes in B cells treated with Anti-IgM or CpG alone or together relative to unstimulated cells showed a variety of pathways were affected including those related to cell proliferation and apoptosis, signal transduction, responses to cytokines and cytoskeleton organization (Fig. 4c).

We also quantified by flow cytometry the B cell surface expression of approximately 250 mouse cell surface proteins using a barcoding strategy[19] and BioLegend LegendScreen kit (Fig. 4d). As compared to unstimulated cells, the expression of 63 surface proteins changed significantly upon treatment. We observed synergy (up to 55 fold) between CpG and Anti-IgM which induced increases in 48% of surface proteins; antagonism of Anti-IgM responses by CpG for 9.5% of markers and antagonism of CpG responses by Anti-IgM in 8% of surface proteins. The expression of 30% of surface proteins decreased in response to CpG and/or Anti-IgM. Taken together, these results support the conclusion that signaling through the BCR alone, TLR9 alone or both resulted in distinct outcomes.

We further analyzed the effect of CpG and Anti-IgM on the expression of an early activation marker (CD69) and three cell surface molecules that are critical to B cell antigen presentation and activation of T_H cells, namely MHC class II, CD86 and CD80 (Fig. S4a–g). MHC class II surface expression increased approximately eight- to 10-fold 24 to 48 h after B cells were treated with Anti-IgM alone which was antagonized by the addition of CpG in a TLR9-dependent process (Fig. S4c,f). However, treatment with CpG alone induced a four to five-fold increase in MHC class II surface expression (Fig. S4c,f) indicating that CpG initiates at least two signaling pathways through TLR9, one that antagonizes BCR-induced MHC class II expression and one that independently enhances MHC class II expression. We also determined the effect of CpG treatment on the ability of HEL-specific B cells from MD4 mice to process HEL and present HEL-peptide MHC class II IA^k complexes (HEL-IA^k) on the B cell surface using a HEL- IA^k-specific mAb. After 24 h incubation with HEL, HEL-specific B cells significantly increased the cell surface levels of HEL- IA^k, by approximately 2.5 fold and the addition of CpG blocked this increase (Fig. 4e,f).

Neither CpG nor Anti-IgM treatment had a large impact on CD80 expression at 24 h (Fig. S4b), however, after 48 h, the cell surface expression of CD80 increased approximately two-fold for cells treated with CpG alone, Anti-IgM alone or both, showing neither antagonism

nor synergy (Fig. S4b). In contrast, Anti-IgM treatment induced a large increase in the expression of CD86, that was blocked by CpG (Fig. S4a,e). The regulation of the surface expression of CD69 showed a pattern consistent with a simple additive effect of Anti-IgM and CpG (Fig. S4d,g).

We tested the effects of several inhibitors for kinases in the BCR and TLR9 signaling pathways on the induced expression of MHC class II and CD86. The most consistent effects of the inhibitors were on BCR-induced changes in both MHC class II and CD86 expression although these effects were only partial (Fig. 4g,h). In contrast, the TLR9 induced changes in MHC class II and CD86 expression were unaffected by the inhibitors suggesting the possibility in both cases of redundancy in the signaling pathways.

Taken together, these results provide evidence that signaling through the BCR, TLR9 or both trigger distinct transcriptional programs and have differential effects on expression of cell surface markers. Of greatest interest is the antagonistic effects of TLR9 signaling on BCR-induced increases in expression of peptide-MHC class II complexes and the costimulatory molecule CD86.

CpG blocks B cell-T_H cell interactions in vitro

We determined the effect of CpG on the length of time antigen-specific B and T cells interacted *in vitro* in the presence of antigen. We incubated HEL-specific T cells from 3A9 HEL transgenic I-A^k mice labeled with CMTPX with HEL-specific B cells from MD4 HEL transgenic mice labeled with CMFDA in culture with HEL alone, CpG alone or HEL plus CpG and imaged the cells continuously over a 24 h period at a rate of 1 frame per 10–20 min. HEL induced a significant increase in the duration of colocalization of T cells and B cells which was antagonized by CpG (Fig. 5a). The presence of HEL also resulted in a decrease in both the speed and length of the tracks of T cells that was mitigated by CpG (Fig. 5b,c).

We determined the effect of TLR9 signaling on the ability of antigen-specific B cells to activate antigen-specific T cells *in vitro*. In the presence of HEL-specific MD4 B cells and HEL (at either 0.5 or 2.0 μg/ml), HEL-specific 3A9 T cells were induced to increase expression of CD44 (Fig. 5d, Fig. S4h) and proliferate (Fig. 5e). The addition of CpG to cultures (at either 2.0 or 0.2 μM) significantly reduced both CD44 expression and T cell proliferation. In the absence of B cells, T cells did not respond to neither HEL nor CpG. The ability of CpG to antagonize the activation of HEL-specific T cells by HEL-specific B cells was dependent on the expression of TLR9 by B cells but not on the expression of TLR9 by T cells (Fig. 5f,g). Wild type or TLR9-deficient 3A9 T cells cultured with wild type MD4 B cells and HEL proliferated, and increased expression of CD44, which was blocked by the presence of CpG. In contrast, CpG had no effect on the proliferation and CD44 expression of neither wild type nor TLR9-deficient 3A9 T cells induced by TLR9-deficient MD4 B cells. CpG had no effect on the ability of wild type $CD4^+$ T cells to increase expression of CD44 (Fig. 5h) or proliferate (Fig. 5i) in response to stimulation with anti-CD3 and anti-CD28.

We also tested the effect of CpG on the ability of B cells to respond to and capture HEL from cell surfaces and to process and present it to HEL-specific 3A9 T cells using NIH3T3 cells stably expressing HEL (NIH3T3-HEL) or transduced with a mock vector (NIH3T3-Mock) (Fig. 6a,b). HEL-specific MD4 mouse B cells (but not nonspecific WT B cells) captured HEL detected by flow cytometry using an HEL-specific mAb (Fig. 6c) and increased expression of CD86, MHC Class II and CD69 (Fig. 6d). For both CD86 and MHC class II, the presence of CpG blocked this increase but had a synergistic effect on the increase in CD69 expression (Fig. 6d). Coculture of HEL-specific MD4 B cells and 3A9 T cells in the presence of NIH3T3-HEL cells (but not NIH3T3-Mock cells) resulted in the activation of T cells to proliferate (Fig. 6e) and increase their expression of CD44 (Fig. 6f,g), both of which were reduced in the presence of CpG.

Taken together, these results demonstrate that in the presence of CpG, antigen-specific B cells are unable to present soluble antigen or antigen captured from cell surfaces and activate antigen-specific helper T cells.

The effect of CpG on B cell responses in vivo

To test the effect of CpG on B cell responses *in vivo*, we generated chimeric mice in which the B cells were either WT or MyD88-deficient and all other hemotoepoetic cells were WT (Fig. S5a). The reconstitutions in the two chimeras were similar (Fig. S5b). The MyD88 deficiency in B cells is not predicted to impact the intrinsic ability of B cells to participate in T cell-dependent antibody responses as robust T-dependent antibody responses are elicited by immunization of MyD88 KO mice *in vivo* [11]. We immunized the chimeric mice with alum adsorbed NP-CGG plus CpG, harvested the spleens on day 14 post immunization and analyzed the cells by flow cytometry according to the gating strategy shown (Fig. S5c). Although the spleens of WT chimeras had a larger total number of GC B cells as compared to the spleens of MyD88 KO chimeras (Fig. 7a,b), the percent and total number of GC B cells that were NP-specific were significantly higher in MyD88 KO chimeras as compared to WT chimeras (Fig. 7c,d). Similarly, the total number of IgG-class-switched B cells was higher in WT chimeras as compared to MyD88 KO chimeras (Fig. 7e,f) but the opposite was the case for the percent and total number of NP-specific B cells (Fig. 7g,h). The total number of cells of the PC lineage was greater in WT chimeras as compared to MyD88 KO chimeras (Fig. 7i,j) but the number of NP-specific Ab secreting cells was larger in the spleens of MyD88 KO chimeras as compared to WT chimeras (Fig. 7k,l). We also determined the total number of T_{FH} cells ($CD4^+$ $CXCR5^+$ $PD1^+$) in the spleens of the chimera mice 14 days post immunization and found no significant difference in the T_{FH} cell numbers between the MyD88 KO and WT chimeras, although the WT chimeras tended to have more T_{FH} cells (Fig. S5d,e). However, without the tools to determine the percent of T_{FH} cells that were antigen specific, this observation is difficult to interpret given the differences observed for total versus antigen-specific GC B cells, isotype switched B cells and PCs (Fig. 7).

Chimeras containing WT B cells showed higher NP-specific IgM serum responses as compared to chimeras containing MyD88 KO B cells (Fig. 7m). For total NP-specific IgG, although the peak levels at day 30 post immunization were not significantly different in

immunized chimeras (Fig. 7n), the NP-specific IgG levels in chimeras containing WT B cells dropped faster than those containing MyD88 KO B cells. The most dramatic differences were in the levels and persistence of high-affinity NP-specific IgG (Fig. 7o) that reached higher peak levels and persisted for weeks longer in chimera containing MyD88 KO B cells as compared to those containing WT B cells (Fig. 7o). Thus, CpG drives IgM production and short-lived antigen-specific IgG responses that do not affinity mature *in vivo*.

The effect of CpG on antibody affinity in humans

We previously carried out a longitudinal study of the Ab response to a candidate malaria vaccine administered with or without CpG to healthy malaria-naïve individuals in the U.S. (www.clinicaltrials.gov NCT no: NCT00320658) [20]. The vaccine was composed of the recombinant *Plasmodium falciparum* protein, apical membrane protein 1 (*Pf*AMA1) formulated on Alhydrogel and mixed with 564 μg of CpG 7909. We determined that the inclusion of CpG in the vaccine resulted in significantly higher AMA1-specific IgG titers but did not have an impact on the longevity of the responses [20].

Here, using serum samples from that trial, we determined the effect of the inclusion of CpG in the vaccine on the affinity of the IgG response. Sera were collected from 10 individuals who received the vaccine alone and 10 who received the vaccine containing CpG 70 days post vaccination and IgG was purified on Protein G columns (Fig. 8). The chromographic profiles of the IgG from all individuals were similar and IgGs appeared highly pure (Fig. 8a). The purified IgGs were analyzed by BIACore with *Pf*AMA1 recombinant protein adsorbed to CM5 chips. There was no difference in the apparent affinities (Fig. 8b,c) or the off rates (Fig. 8b,d) between the individuals who received the vaccine alone or the vaccine containing CpG. Thus, although the inclusion of CpG resulted in an increase in the levels of antigen-specific antibody [20], CpG caused no detectable increase on the affinity of these antibodies.

DISCUSSION

It was established over thirty years ago that the processing and presentation of antigen to $CD4^+$ T_H cells by antigen-specific B cells is highly efficient [21]. However, although it was clear that antigen-specific B cells were able to efficiently process and present antigen, the role of B cell antigen processing and presentation in T cell-dependent antibody responses was not elucidated until recently. Several studies have now provided evidence that the ability of B cells to process and present antigen to antigen-activated T_H cells and to T_{FH} cells provides critical check points for the entry of B cells into the GC and for affinity selection of B cells expressing somatically hypermutated Ig genes in the GC [1, 2, 3, 4]. The quality of the B cell's presentation of antigen to antigen-activated T cells at the T cell-B cell border in lymphoid organs determines, in part, if a B cell will enter the GC or differentiate along a GC-independent pathway to become short-lived plasma cells or GC-independent memory B cells [2]. In the GC light zone selection by T_{FH} cells is dependent on the density of MHC peptide complexes on the B cell surface, reflecting the B cell's affinity-dependent ability to compete for antigen capture from FDCs [3]. Thus, B cell antigen processing and presentation controls, to a large extent, B cell clonal selection.

Given the central role of B cell antigen gathering, processing and presentation in the generation of high affinity, long-lived antibody responses, it is likely that this B cell function is regulated to ensure appropriate and timely responses to antigenic challenge, particularly during infection. However, little is known about the role of innate immune receptors that respond to PAMP-containing microbial products in regulating these processes. We show that TLR9 signaling promotes B cell proliferation and differentiation into antibody secreting cells as previously shown [7, 22, 23] and in addition triggers changes in gene expression including the downregulation of BCL6, a transcriptional repressor of PC differentiation, and upregulation of BLIMP1, a transcription factor that promotes PC differentation. However, TLR9 signaling greatly diminished the ability of antigen-specific B cells to gather, process and present antigen, and to interact with and activate antigen-specific $CD4^+$ T cells *in vitro*. In the presence of CpG, antigen-specific B cells also fail to upregulate important costimulatory ligands for T cells, including CD86. The ability of CpG to diminish the ability of B cells to capture antigen from membranes and cell surfaces—as was shown here—is particularly relevant to the regulation of B cell responses *in vivo* where the B cells in lymphoid organs access most antigens on the surfaces of FDCs [24].

These findings have implications for the outcome of T cell-dependent antibody responses *in vivo*. If during an infection B cells encounter TLR9 ligands, our data suggest that the B cells would have diminished ability to gather, process and present antigen to antigen-activated T_H cells at the T-B border of lymphoid organs. As a consequence, B cells would be directed to GC-independent pathways, yielding affinity unselected plasma cells and GC-independent memory B cells. It may be advantageous to rapidly produce antibodies with a wide range of affinities in response to TLR9 activation during an acute infection and to leave an unselected broad B cell repertoire for future antigen challenge [2]. Such a mechanism may underlie a recent observation in a nonhuman primate model, that although adjuvants that stimulate innate immune receptors, including TLRs, were effective in enhancing the magnitude of Ab responses to protein immunogens, remarkably, these were not able to increase SHM [13].

We present evidence both in mice and in humans consistent with this model. We compared the responses of chimeric mice containing B cells that were WT to the responses of chimeric mice containing MyD88 KO B cells upon immunization with an alum adsorbed protein antigen (NP-CGG) given together with CpG. The ability of B cells to respond to CpG resulted in short-lived low-affinity IgG responses and reduced numbers of antigen-specific GC B cells. In humans we provided evidence that the inclusion of CpG in a recombinate protein vaccine formulated on alum resulted in increased levels of antigen-specific Abs but had no detectable effect on the apparent affinity of the antibodies as compared to the response of individuals receiving the vaccine alone. To our knowledge the studies presented here and those of Francica *et al.* [13] are the only ones to address the impact of TLR ligands as adjuvants on antibody affinity maturation. It will be of genuine interest to determine the generality of these findings to other vaccines and vaccine regimens.

METHODS

Mice

C57BL/6, B10.BR-H2K2H2-T18a/SgSnJArc, B cell-deficient (B6.129S2-Ighm^{tm1Cgn}/J) (μMT) mice, B6.129S2-Ighmtm1Cgn/J, MyD88 KO mice and B6 CD45.1 congenic WT mice were purchased from Jackson Laboratory. HEL- specific BCR transgenic mice (MD4) [25], were purchased from Taconic Farms. TLR-9 deficient mice were provided by S. Akira (Osaka University, Osaka, Japan). HEL-specific, MHC class II I-A^k restricted TCR transgenic mice (3A9) [26], were provided by I.Gery (NEI/NIH, Bethesda, MD, USA). Both MD4 and 3A9 mice were kept hemizygous for the transgenic alleles in a MHC class II I-A^k or I-A^b haplotype by crossing 3A9 or MD4 mice with wild-type mice of the relevant haplotype. TLR9-deficient MD4 and 3A9 mice were generated by crossing the MD4 and 3A9 mice with TLR9-deficient mice for at least three generations. TLR9-deficient mice on the MHC class II I-A^k haplotype were generated as the F2 generation of a cross between TLR9-deficient mice (I-A^b) and B10.BR-H2K2H2-T18a/SgSnJArc (I-A^k) mice. These TLR9-deficient mice were further crossed (at least four generations) MD4 or 3A9 mice crossed with I-A^k haplotypes to obtain TLR9-deficient MD4 or 3A9 mice in I-A^k haplotype. Mice were bred and maintained in NIH animal facility according to Animal Care and Use Committee Standards.

Antibodies and proteins

Abs specific for mouse: CD19 (Clone:6D5) (conjugated to Alexa488, Alexa700, BV650, PeCy7 or BV421); CD45R/B220 (Clone:RA3-6B2) (conjugated to PE, Alexa488, Alexa647, Alexa700, BV421, BV785, BV605 or BV510); CD80 (Clone:16-10A1) (conjugated to Alexa647); CD86 (Clone: GL1) (conjugated to PERCP, PERCP-Cy5.5 or Alexa488); IgM (Clone:RMM-1) (conjugated to BV605); CD69 (Clone: H1.2F3) (conjugated to PE or BV605); CD4 (Clone:RM4-5) (conjugated to Alexa 488 or BV605); CD44 (Clone:IM7) (conjugated to Alexa700 or Alexa647); MHC class II I-A^b (Clone:KH74) (conjugated to Alexa488); MHC class II I-A^k (Clone: 10–3.6)(conjugated to PE); IgG1 (Clone: RMG1-1) (conjugated to biotin or Alexa647) and IgG2a (Clone:RMG2a-62) (conjugated to Alexa647), CD138 (Clone:281-2) (conjugated to PE), CD45.2 (Clone:104) (conjugated to BV650 or APC), CD45.1(Clone:A20) (conjugated to Alexa700, Alexa488 or APC), CD3e (Clone: 145-2C11), CD28 (Clone:37.51) and streptavidin (PE conjugated) were purchased from BioLegend. Isotype control-mouse IgG1 (Clone:MG1-45) and IgG2a (Clone:MG2a-53) were purchased from BioLegend. Abs specific for: p-Btk (p-Y223) (Clone:N35-86) (conjugated to PE); pMAPK/p38 (pT180/pY182) (Clone:36/p38) (conjugated to Alexa647); p-Syk (pY352) (Clone: 17A/P-ZAP70) (conjugated to Alexa488); pAkt (pS473) (Clone:M89-61) (conjugated to Alexa647); H2-M (Clone: 2E5A) (unconjugated) and CD71 (unconjugated) (Clone C2F2) and, anti-mouse IgD (Clone:11-26c.2a) conjugated to BV786 were purchased from BD Biosciences. Polyclonal F(ab′)$_2$ anti-mouse IgG (conjugated to Alexa647 or Alexa488) and polyclonal F(ab′)$_2$ anti-mouse IgM (unconjugated and conjugated to Alexa647) were purchased from Jackson ImmunoResearch. Abs specific for mouse CD95 (Clone:15A7) (conjugated to Percp e710) and mouse IgM Clone:eb121-15F9) (conjugated to e450) were purchased from ThermoFisher. Abs specific for LAMP-1 (Clone: 1D4B) were purchased from Santa Cruz Biotechnologies. PE conjugated NP was purchased

from Biosearch Technologies. The mouse mAb (OX68) specific for the third and fourth domains of rat CD4, as described [27], was provided by N. Barclay (University of Oxford, Oxford UK). The hybridoma secreting mouse mAb (AW3.18) specific for the HEL peptide (residues 48-62)-MHC Class II A^k complex [28], was provided by P. Roche (NCI/NIH, Bethesda, MD, USA) and purified antibody was produced by L. Lantz (NIAID/NIH, Rockville, MD,USA). The mouse mAb (F10.6) specific for HEL [29], was provided by J. Charles-Guery and D. Hudrisier (University of Toulouse, Toulouse, France). Fluorescent labeling of the unconjugated Abs was done using a LYNX kit purchased from Bio-Rad.

Flow cytometry

Flow cytometry was performed on a BD LSRII flow cytometer and data were analyzed in Flowjo software (Tree Star, Inc.). During analysis, dead cells were excluded by staining with LIVE/DEAD fixable dead cell stain kits (ThermoFisher).

Cells

B cells and naïve $CD4^+$ T cells were isolated from mouse spleen using mouse B cell and naïve T cell isolation kits (Miltenyi Biotech) according to previously published optimized protocols [30, 31]. NIH3T3 mouse fibroblast cell line (ATCC CRL-1658) was provided by O. Voss. Phoenix Eco retroviral packaging cell line (ATCC CRL-3214) was purchased from American Type Culture Collection (ATCC). All cells were maintained in RPMI 1640 media supplemented with 50 μM 2-mercaptoethanol, 50 U/ml penicillin, 50 μM streptomycin, 2 mM L-glutamine, 0.1 mM non-essential amino acids, 1 mM sodium pyruvate and 10 mM HEPES unless otherwise specified. The pathway inhibitors SP600125, PD98059, Wortmannin, Rapamycin, SB202190 were purchased from Invivogen. MHY1485 and Akt Inhibitor IV (Akt IV) were purchased from Sigma-Aldrich.

B cell–T cell co-cultures

B cells were isolated from the spleens of MD4 mice on the MHC Class II I-A^k haplotype. Naïve T cells were isolated from the spleens and lymph nodes of 3A9 mice. Both cells were labeled with Cell Proliferation Dye eFluor® 450 (ThermoFisher) and mixed at 1:1 ratio (7.5×10^4 each) in complete media and incubated in 96-well plates at 37 °C in the presence of HEL (1 μg/ml) and/or CpG (1 μM). Stimulation by membrane bound antigens was carried out by incubating NIH3T3 cells HEL or mock transfected in 96-well plates, 5×10^4 cells/well, one day before adding the B cell–T cell mixture.

Visualization of real time interactions between B and T cells was carried out by labeling B cells and T cells with CellTracker™ Green CMFDA and CellTracker™ Red CMTPX Dyes (ThermoFisher) respectively. Labeled cells were plated into 48-well plates at 1:1 ratio (1×10^5 each) and stimulated as indicated above. Interaction between cells were recorded as 10–20 min time-lapse photos by IncuCyte ZOOM system (Essen Bioscience) for 24 h. Image analysis was performed using Imaris Software.

Human Study Population and Vaccination Procedures

Serum was obtained 70 days post immunization from malaria naïve adults enrolled in a phase 1 clinical trial of the blood stage malaria vaccine candidate, 80 μg of AMA1-C1,

formulated on Alhydrogel and mixed with 564 μg of CpG 7909[32] (www.clinicaltrials.gov no. NCT00320658) as detailed elsewhere [33]. The trial was conducted under Investigational New Drug Applications reviewed by the U.S. Food and Drug Administration and was reviewed and approved by the National Institute of Allergy and Infectious Diseases Review Board and by the University of Rochester Institutional Review Board and funding agency. Written informed consent was obtained from all participants. Serum samples from 20 individuals were randomly selected for analysis, half of whom had been vaccinated with CpG7909-containing vaccine and half with the vaccine alone.

Generation of stable cell lines expressing HEL chimeric protein

NIH/3T3 cells, stably expressing HEL on their surface, were generated by transfection with a construct encoding a protein chimera containing on its N-terminus the entire HEL protein (Accession no: AAA48943.1) followed by a serine-tyrosine linker sequence and then by the third and fourth transmembrane and intracellular domains of rat CD4 (residues 206-457) (Accession no: P05540.1). A codon optimized final construct was generated by Geneart Gene Synthesis, (ThermoFisher) which was then subcloned into a pFB-Hygro retroviral vector[34]. Transduction of NIH/3T3 cells using the Phoenix-Eco system and selection of the stably transfected cells were done as previously described[35].

Bone marrow chimeras and immunizations

To generate B cell lineage-specific TLR9-deficient mice, lethally irradiated 7–8 weeks old C57BL/6 mice (CD45.1 haplotype) were reconstituted with 10^7 bone marrow cells of which 90% were from μMT mice and 10% were from either MyD88-deficient or WT mice. Mice were allowed to reconstitute for at least 8 weeks before immunization with both 100 μg NP(15)CGG (Biosearch Technologies) adsorbed into 100 μl Alum (ThermoFisher) in PBS and 65 μg CpG B (ODN 1826) (Invivogen) in PBS intraperitoneally.

Signaling pathway analyses

B cells isolated from mouse spleen were cultured in 96 well plates at 37 °C with the appropriate stimulus. At each time point, cells were fixed with 4% PFA containing HBSS buffer for 10 min at 37 °C followed by permeabilization on ice using pre-chilled Perm Buffer III (BD Biosciences) for 30 min. Cells cultured with different stimuli were barcoded by staining with B220 antibodies conjugated with different fluorochromes. Following barcoding as described in[19], samples from the same time point, each having unique B220 staining patterns, were pooled in one well for intracellular staining using phospho-kinase specific Abs. For flow cytometry each sample was gated based on the barcodes. For each phospho-specific-Ab, the net mean fluorescence intensities (MFI) was calculated by subtracting the MFI of the fluorescence minus one (FMO) control from the MFI of the actual samples. Fold change in the phosphorylation content was determined as the ratio of the net MFI of a stimulated condition to the net MFI of the unstimulated sample at the same time point. Changes in calcium influx into the cell as a response to different stimulation conditions were analyzed using Fluo-4 and Fura red dyes (ThermoFisher) as explained in[20].

Characterization of BCR-mediated antigen internalization

To quantify internalization of antigen from solution, B cells isolated from HEL-specific BCR transgenic mice (MD4) were incubated with saturating amounts (4 μg/ml) of soluble HEL (Sigma-Aldrich) on ice for 30 min. Unbound antigen was removed by repeated washes at 4°C. Cells were cultured in complete media with or without CpG at 37 °C and aliquots were taken with time and transferred to ice cold FACS buffer (HBSS supplemented with 5% FCS, 10 mM HEPES and 10 mM sodium azide). Cells were stained with Alexa647-conjugated antibody specific for mouse IgM and analyzed by flow cytometry. Downmodulation of the surface BCR was measured using the following formula: receptor downmodulation % = 100 X [net MFI (t_x) / net MFI (t_0)].

Alternatively, B cells isolated C57BL/6 mouse spleens were incubated on ice with Alexa647-conjugated Anti-IgM for 30 min, then washed and cultured at 37 °C for increasing lengths of time. At each time point aliquots were transferred into ice cold RPMI1640 supplemented with BSA (0.5%) either at pH 7.4 or at pH 2.5 to strip surface bound Anti-IgM. Following fixation with 4% PFA, cells were analyzed by flow cytometry and the portion of BCR internalized was determined using the following formula: Internalized BCR %= 100X [net stripped MFI (t_x) − net stripped MFI of 0 minutes time point] / [net non-stripped MFI (t_x) − net stripped MFI (t_0)].

To characterize the pH of the intracellular compartment into which the BCR-bound HEL was internalized, a pH sensitive fluorescent dye pHrodo Red Avidin (ThermoFisher) was conjugated to biotinylated HEL (SigmaAldrich) according to manufacturer's guidelines. B cells isolated from MD4 mice were incubated on ice with pHrodo-HEL for 30 min, and then washed and cultured at 37 °C for increasing lengths of time in phenol red-free RPMI complete media (Gibco-ThermoFisher) with or without CpG. At each time point aliquots were analyzed with flow cytometry to determine both the increase in total internalized pHrodo-HEL and the decrease in pH of the endosomal compartment.

Preparation of antigen-containing lipid bilayers and membrane sheets

Planar lipid bilayers (PLBs) were prepared as described [36]. Briefly, PLB containing biotin lipid were formed on the acid-cleaned glass bottom of an 8-well lab-tek-chamber from 10 μM small unilamellar vesicles consisting of DOPC and DOPE-cap-biotin (Avanti Polar Lipids). HEL was incorporated into the PLB by adding 10 nM Alexa Fluor 488-labeled biotinylated HEL into PLB-containing chambers, incubating for 30 min at RT, and then washing to remove unbound HEL.

Plasma membrane sheets (PMS) were prepared as described [37]. Briefly, 1.5×10^5 293A cells were seeded into a chamber of an 8-chamber Lab-Tek II chambered #1.5 German coverglass system (Nunc) and cultured overnight. The chambers were filled with blocking solution (HBSS containing 2% BSA and 2.5 mM Ca^{2+}) and the cells were sonicated with a 130 watt, 20 kHz probe-typed ultrasonic processor at 22% Amp for 5 s at a time by placing the probe right beneath the top of buffer. To tether antigen on the PMS, PMS were incubated sequentially for 30 min with 0.5 μg/mL biotinylated Annexin V (Biolegend), 5 μg/ml Streptavidin (Invitrogen) and 50 nM Alexa Fluor 488-conjugated biotinylated HEL with

washing between additions with 15 ml buffer (1 × HBSS containing 0.2% BSA and 2.5 mM Ca^{2+}).

Imaging and image analyses of B cells responding to membrane-bound antigen

To image BCR clustering and antigen recruitment to the contact area between cells and PLBs and PMSs, time-lapse live cell total internal reflection fluorescence (TIRF) imaging was performed using an Olympus IX-81 (Olympus) equipped with a TIR controlling system, EMCCD camera and × 100 objective lens (Olympus) controlled by Metamorph software (Molecular Devices) as detailed elsewhere [38, 39, 40]. Time lapse live-cell imaging was done at 37 °C on a heated stage with an objective lens heater and a heating chamber with image acquisition at 2 s intervals for 20 min. All acquired images were background-subtracted before further analysis. For the analysis of BCR accumulation in the contact area with time after the cells contacted the PLBs or PMSs, the fold change in intensity was calculated by the mean fluorescence intensity (MFI) of the BCR in the contact area at each time point divided by the MFI of the first BCR cluster appeared on the field after setting the threshold above background signal using Image Pro Plus (Media Cybernetics) software. For analysis of antigen recruitment into the contact area with time after the cells contacted the PLBs or PMSs, the fold change in intensity was calculated by the MFI of antigen in the cell contact area at a given time point divided by the MFI of antigen before the B cell contacted the PLB- or PMS-containing fluorescence-labeled antigen.

For the acquisition of three color confocal *z* stack images, ZEISS 780 LSM confocal microscope (ZEISS) with × 63 1.45 NA oil objective lens was used with three laser lines, 488, 561, and 633 nm at the optimal 240 nm interval to the *z* direction as described [41]. Briefly, MD4 mouse splenic B cells were labeled with DyLight649-conjugated goat Fab fragment specific for IgM and put into a chamber containing CM-DiI-labeled PMS bearing AlexaFluo488-labeled antigen at 37 °C for 30 min in the presence or absence of CpG and fixed with 4% PFA. *z*-stack three color channel images were acquired of the whole cells on the PMS to obtain the spatial information of internalized antigen, membrane and the BCR. To quantify the percentage of antigen internalization or total fluorescence intensity (TFI) of internalized antigen, Matlab software (Mathworks) and the Matlab code obtained from Dr. P. Tolar (The Francis Crick Institute, London, UK) were used as described in detail [37] after splitting three channel images into single channel image using Image J. Internalized antigen was quantified after defining the surface of PMSs according to the code. Briefly, two channel confocal *z*- stack images for antigen and membrane were separated using Image J program and saved as tif files for the use of this Matlab code. Using the code, antigen-incorportaed PMS outside the cell contact area was considered as background ROI and MFI of the background area was obtained to exclude scattered fluorescence from the surface antigen of PMS. To distinguish the internalized antigen from the surface antigen, surface plane of the PMS from *z*-stack series was determined. ROIs including whole cell area were drawn on the base of DIC images and were determined the percentage of antigen internalization or total fluorescence intensity (TFI) of internalized antigen. For the 3D image reconstitution and 3D Pearson's colocalization analyses, Imaris software (Bitplane, Belfast, UK) was used as described [41]. To obtain the colocalization coefficient from internal compartments of the cells, only *z*- slices above the PMS surface determined by Matlab code

described earlier were used for the 3D reconstitution and calculation of 3D Pearson's colocalization coefficient between internalized antigen and membrane taken from the PMS or between the internalized antigen and BCR.

Confocal microscopy

Splenic B cells, purified from MD4 transgenic mice were attached to poly L-Lysine coated cover glass. Cells were incubated at 37 °C in complete media containing Rhodamine-conjugated HEL (Nanocs) with or without CpG for increasing time. Cells were fixed with fixation buffer (4% PFA in PBS at 37 °C) for 10 min, permeabilized with PBS containing 0.5% Saponin and 5% BSA at RT for 20 min, washed and incubated with PBS containing 10% normal rat serum and 0.5% Saponin at RT for 1 h. Cells were stained with fluorescent mAb specific for CD71, LAMP1 and H2M and staining for early ($CD71^+$) and late ($LAMP1^+$) endosome as well as for antigen processing compartment ($H2M^+$) using fluorescently labeled monoclonal antibodies diluted in blocking buffer mounted on microscope slides using ProLong Gold Antifade mountant with DAPI (Thermofisher). Zeiss LSM780 microscope equipped with 63X A Zeiss Plan-Apochromat 633 oil-immersion. Objective was used for image acquisition. 3D Colocalization of Rhodamine-HEL with the fluorescent antibodies was calculated using Imaris software.

Electron microscopy

For transmission electron microscopy (TEM) and electron tomography (ET), B cells were fixed by suspending in modified Karnovsky's fixative prepared with 10 ml PFA (4%), 20 ml Sodium Phosphate Buffer (0.2 M), 2 ml Glutaraldehyde (50%) and 8 ml distilled water (Electron Microscopy Sciences) and processed using microwave irradiation as previously described,[42] with the following exceptions: Between each step, cells were recovered by centrifugation for 5 min at 800×*g*. Fixed and dehydrated cells were infiltrated with Araldite resin (SPI Inc). Sections for tomography were cut at a thickness of 200 nm, and imaged without post-section staining. Tomographic tilt series were collected on an Ultrascan 4000 camera (Gatan, Inc., Pleasanton, CA), using SerialEM acquisition and control software (University of Colorado, Boulder, CO).[43] Volumetric reconstructions were performed using the Batchruntomo script (University of Colorado). Particle counts and volumetric measurements were conducted using IMOD software (University of Colorado). [44] Volumetric models were rendered using Amira for Biosciences (FEI Inc.).

ELISAs and ELISPOT

Concentrations of cytokines (IL-2, IL6, IL10 and TNF) and immunoglobulins (IgG and IgM) secreted by purified splenic B cells in culture were measured by analyzing the supernatants with relevant Ready-Set-Go! ELISA kits (ThermoFisher) according to manufacturer's guidelines.

The relative affinities of NP-specific antibodies were determined by applying 100 μl diluted mouse serum (1/1000 to 1:100000) onto Nunc MaxiSorp® 96 well flat bottom plates (ThermoFisher) previously coated with 10 μg per well of either NP4-BSA (to capture high affinity antibodies) or NP30-BSA (to capture diverse affinity antibodies) (Biosearch Technologies). Plates were washed and bound IgG was detected using HRP-conjugated anti-

IgG (Jackson ImmunoResearch) developed with 3,3′,5,5′-tetramethylbenzidine (TMB) substrate (ThermoFisher). The reaction was quenched using a stop reagent purchased from Sigma-Aldrich.

The OD at 450 nm was measured on a Spectramax plate reader (Molecular Devices). ELISPOT analysis of NP specific antibody secreting cells were carried out according to the protocol explained elsewhere[10] and plates were evaluated and imaged by Zellnet Consulting.

Quantitative RT-PCR (qPCR) and RNA sequence analyses

For qPCR analyses, RNA was isolated from mouse splenic B cells stimulated *in vitro* using RNeasy mini or micro Kits (Qiagen) according to manufacturer's guidelines. cDNA was generated using iScript™ Reverse Transcription Supermix (Bio-Rad). qPCR assays containing primers and Taqman probes were purchased from Integrated DNA Technologies, qPCR assays containing primers only were purchased from Eurofins MWG Operon. Sequences of these primers and probes are listed in Supplemental Table 1. iQ™ SYBR® Green Supermix (Biorad) or Platinum® Quantitative PCR SuperMix-UDG (ThermoFisher) were used for amplification of target genes. Fold change in gene expression (target vs control) was calculated as previously shown in [45].

For RNA sequencing, 250 μl of purified mouse B cells cultured in full media for 4 h were mixed with 750 μl of Trizol LS (Thermofisher) and RNA was isolated according to manufacturer's recommendations. Total RNA was prepared for Next Generation Sequencing (NGS) using the TruSeq Stranded mRNA-Seq library preparation kit (Illumina). Quality and size of the final purified libraries were tested on BioAnalzyer DNA 1000 chips (Agilent Technologies.). Libraries were quantified by qPCR using the Kapa Quantification Kit for Illumina sequencing (Kapa Biosystems) and then normalized to 2.0 nM stocks. These samples were pooled equally and clustered on the HiSeq 2500 (Illumina) using 12 pM of template for a 2x100 bp Rapid sequencing run. Raw NGS reads were prepped by first removing any illumina adapter sequences using Cutadapt v1.12 [46], and then trimmed and filtered for quality, q=18, and length, min length 35bp using FastX Tool Kit v0.0.13 (Hannon Lab, Cold Spring Harbor Laboratory). Trimmed reads for each replicates were then mapped to Mus musculus mm10 genome using Tophat2 v2.1.1 [47] set to report only matched pairs. Final transcripts based on the combined replicates and then differentials for each comparison were generated using Cufflinks [47] suite using pooled normalization for each experimental condition. Changes in the transcriptional regulation of various pathways were analyzed using Ingenuity Pathway Analysis Software (Qiagen).

Purification and Surface plasmon resonance(BIAcore) binding analysis of Anti-PfAMA1 antibodies

Total serum IgG antibodies from Pf AMA1 immunized patient subjects were purified by protein G affinity chromatography. Briefly, 0.5 ml serum from each individual subject was loaded onto a 5 ml HiTrap Protein G column (GE healthcare) and subjected to a standard elution with a glycine pH gradient. The eluted IgG protein was pooled together and dialyzed against 10 mM Hepes(pH 7.5) and 0.15 M NaCl for binding studies.

Surface plasmon resonance measurements were performed using a BIAcore 3000 instrument and analyzed with BIAevaluation 4.1 software (Biacore AB). To measure the affinity, Pf AMA1 protein was immobilized on caboxylated dextran CM5 chips (Biacore AB) to 500–1500 response units (RU) using a primary amine-coupling and 10 μl/min flow rate in 10mM sodium acetate (pH 4.5). The analyte consisted of serial dilutions of IgG antibodies between 16.0 and 75 nM in a buffer containing 10 mM HEPES (pH 7.4) and 0.15 M NaCl. The dissociation constants were obtained by kinetic curve fitting using BIAevaluation 4.1 (BIAcore Inc.).

Statistical Analyses

Statistical significance between different experimental groups were measured using GraphPad Prism software. The methods used for each experiment and the *P* value ranges were indicated in the relevant figure legends.

Data availability statement

Additional details of the experimental procedures can be found in the Life Sciences Reporting Summary. The data that support the findings of the study are available from the corresponding author upon request. RNA seq data was uploaded to SRA database under project number: PRJNA422889.

Supplementary Material

Refer to Web version on PubMed Central for supplementary material.

Acknowledgments

This work was supported by the Intramural Research Program of the National Institutes of Health, National Institute of Allergy and Infectious Diseases. Authors thank Dr. Joseph Brzostowski and Dr. Silvia Bolland for their helpful suggestions. Authors declare no competing financial interests.

References

1. De Silva NS, Klein U. Dynamics of B cells in germinal centres. Nat Rev Immunol. 2015; 15:137–148. [PubMed: 25656706]
2. Kurosaki T, Kometani K, Ise W. Memory B cells. Nat Rev Immunol. 2015; 15:149–159. [PubMed: 25677494]
3. Mesin L, Ersching J, Victora GD. Germinal Center B Cell Dynamics. Immunity. 2016; 45:471–482. [PubMed: 27653600]
4. Bannard O, Cyster JG. Germinal centers: programmed for affinity maturation and antibody diversification. Curr Opin Immunol. 2017; 45:21–30. [PubMed: 28088708]
5. DeFranco AL, Rookhuizen DC, Hou B. Contribution of Toll-like receptor signaling to germinal center antibody responses. Immunol Rev. 2012; 247:64–72. [PubMed: 22500832]
6. Rawlings DJ, Schwartz MA, Jackson SW, Meyer-Bahlburg A. Integration of B cell responses through Toll-like receptors and antigen receptors. Nat Rev Immunol. 2012; 12:282–294. [PubMed: 22421786]
7. Akkaya M, et al. B Cells Produce Type 1 IFNs in Response to the TLR9 Agonist CpG-A Conjugated to Cationic Lipids. J Immunol. 2017; 199
8. Roche PA, Furuta K. The ins and outs of MHC class II-mediated antigen processing and presentation. Nat Rev Immunol. 2015; 15:203–216. [PubMed: 25720354]

9. Rookhuizen DC, DeFranco AL. Toll-like receptor 9 signaling acts on multiple elements of the germinal center to enhance antibody responses. Proc Natl Acad Sci U S A. 2014; 111:E3224–3233. [PubMed: 25053813]
10. Akkaya M, et al. T cell-dependent antigen adjuvanted with DOTAP-CpG-B but not DOTAP-CpG-A induces robust germinal center responses and high affinity antibodies in mice. Eur J Immunol. 2017
11. Gavin AL, et al. Adjuvant-enhanced antibody responses in the absence of toll-like receptor signaling. Science. 2006; 314:1936–1938. [PubMed: 17185603]
12. Coffman RL, Sher A, Seder RA. Vaccine adjuvants: putting innate immunity to work. Immunity. 2010; 33:492–503. [PubMed: 21029960]
13. Francica JR, et al. Analysis of immunoglobulin transcripts and hypermutation following SHIV(AD8) infection and protein-plus-adjuvant immunization. Nature communications. 2015; 6:6565.
14. Basso K, Dalla-Favera R. Roles of BCL6 in normal and transformed germinal center B cells. Immunol Rev. 2012; 247:172–183. [PubMed: 22500840]
15. Fleire SJ, et al. B cell ligand discrimination through a spreading and contraction response. Science. 2006; 312:738–741. [PubMed: 16675699]
16. Weber M, et al. Phospholipase C-gamma2 and Vav cooperate within signaling microclusters to propagate B cell spreading in response to membrane-bound antigen. J Exp Med. 2008; 205:853–868. [PubMed: 18362175]
17. Tolar P, Sohn HW, Liu W, Pierce SK. The molecular assembly and organization of signaling active B cell receptor oligomers. Immunol Rev. 2009; 232:34–41. [PubMed: 19909354]
18. Liu W, Meckel T, Tolar P, Sohn HW, Pierce SK. Intrinsic properties of immunoglobulin IgG1 isotype-switched B cell receptors promote microclustering and the initiation of signaling. Immunity. 2010; 32:778–789. [PubMed: 20620943]
19. Akkaya B, et al. A Simple, Versatile Antibody-Based Barcoding Method for Flow Cytometry. J Immunol. 2016; 197:2027–2038. [PubMed: 27439517]
20. Crompton PD, et al. The TLR9 ligand CpG promotes the acquisition of Plasmodium falciparum-specific memory B cells in malaria-naive individuals. J Immunol. 2009; 182:3318–3326. [PubMed: 19234231]
21. Lanzavecchia A. Antigen presentation by B lymphocytes: a critical step in T-B collaboration. Curr Top Microbiol Immunol. 1986; 130:65–78. [PubMed: 3490955]
22. Eckl-Dorna J, Batista FD. BCR-mediated uptake of antigen linked to TLR9 ligand stimulates B-cell proliferation and antigen-specific plasma cell formation. Blood. 2009; 113:3969–3977. [PubMed: 19144984]
23. Genestier L, et al. TLR agonists selectively promote terminal plasma cell differentiation of B cell subsets specialized in thymus-independent responses. J Immunol. 2007; 178:7779–7786. [PubMed: 17548615]
24. Hoogeboom R, Tolar P. Molecular Mechanisms of B Cell Antigen Gathering and Endocytosis. Curr Top Microbiol Immunol. 2016; 393:45–63. [PubMed: 26336965]
25. Mason DY, Jones M, Goodnow CC. Development and follicular localization of tolerant B lymphocytes in lysozyme/anti-lysozyme IgM/IgD transgenic mice. Int Immunol. 1992; 4:163–175. [PubMed: 1622894]
26. Ho WY, Cooke MP, Goodnow CC, Davis MM. Resting and anergic B cells are defective in CD28-dependent costimulation of naive CD4+ T cells. J Exp Med. 1994; 179:1539–1549. [PubMed: 7909325]
27. Akkaya M, Kwong LS, Akkaya E, Hatherley D, Barclay AN. Rabbit CD200R binds host CD200 but not CD200-like proteins from poxviruses. Virology. 2015; 488:1–8. [PubMed: 26590792]
28. Dadaglio G, Nelson CA, Deck MB, Petzold SJ, Unanue ER. Characterization and quantitation of peptide-MHC complexes produced from hen egg lysozyme using a monoclonal antibody. Immunity. 1997; 6:727–738. [PubMed: 9208845]
29. Cauerhff A, Goldbaum FA, Braden BC. Structural mechanism for affinity maturation of an anti-lysozyme antibody. Proc Natl Acad Sci U S A. 2004; 101:3539–3544. [PubMed: 14988501]

30. Traba J, Miozzo P, Akkaya B, Pierce SK, Akkaya M. An Optimized Protocol to Analyze Glycolysis and Mitochondrial Respiration in Lymphocytes. J Vis Exp. 2016
31. Akkaya B, et al. Ex-vivo iTreg differentiation revisited: Convenient alternatives to existing strategies. Journal of immunological methods. 2016
32. Mullen GE, et al. Phase 1 trial of AMA1-C1/Alhydrogel plus CPG 7909: an asexual blood-stage vaccine for Plasmodium falciparum malaria. PLoS One. 2008; 3:e2940. [PubMed: 18698359]
33. Crompton PD, et al. The TLR9 ligand CpG promotes the acquisition of Plasmodium falciparum-specific memory B cells in malaria-naive individuals. J Immunol. 2009; 182:3318–3326. [PubMed: 19234231]
34. Tomlinson DC, L'Hote CG, Kennedy W, Pitt E, Knowles MA. Alternative splicing of fibroblast growth factor receptor 3 produces a secreted isoform that inhibits fibroblast growth factor-induced proliferation and is repressed in urothelial carcinoma cell lines. Cancer Res. 2005; 65:10441–10449. [PubMed: 16288035]
35. Akkaya M, Aknin ML, Akkaya B, Barclay AN. Dissection of agonistic and blocking effects of CD200 receptor antibodies. PLoS One. 2013; 8:e63325. [PubMed: 23691022]
36. Sohn HW, Tolar P, Brzostowski J, Pierce SK. A method for analyzing protein-protein interactions in the plasma membrane of live B cells by fluorescence resonance energy transfer imaging as acquired by total internal reflection fluorescence microscopy. Methods Mol Biol. 2010; 591:159–183. [PubMed: 19957130]
37. Natkanski E, et al. B cells use mechanical energy to discriminate antigen affinities. Science. 2013; 340:1587–1590. [PubMed: 23686338]
38. Liu W, Meckel T, Tolar P, Sohn HW, Pierce SK. Intrinsic properties of immunoglobulin IgG1 isotype-switched B cell receptors promote microclustering and the initiation of signaling. Immunity. 2010; 32:778–789. [PubMed: 20620943]
39. Liu W, Meckel T, Tolar P, Sohn HW, Pierce SK. Antigen affinity discrimination is an intrinsic function of the B cell receptor. J Exp Med. 2010; 207:1095–1111. [PubMed: 20404102]
40. Davey AM, Pierce SK. Intrinsic differences in the initiation of B cell receptor signaling favor responses of human IgG(+) memory B cells over IgM(+) naive B cells. J Immunol. 2012; 188:3332–3341. [PubMed: 22379037]
41. Wang J, Sohn H, Sun G, Milner JD, Pierce SK. The autoinhibitory C-terminal SH2 domain of phospholipase C-gamma2 stabilizes B cell receptor signalosome assembly. Sci Signal. 2014; 7:ra89. [PubMed: 25227611]
42. Offerdahl DK, Dorward DW, Hansen BT, Bloom ME. A three-dimensional comparison of tick-borne flavivirus infection in mammalian and tick cell lines. PLoS One. 2012; 7:e47912. [PubMed: 23112871]
43. Mastronarde DN. Automated electron microscope tomography using robust prediction of specimen movements. Journal of structural biology. 2005; 152:36–51. [PubMed: 16182563]
44. Kremer JR, Mastronarde DN, McIntosh JR. Computer visualization of three-dimensional image data using IMOD. Journal of structural biology. 1996; 116:71–76. [PubMed: 8742726]
45. Gordon EB, et al. Targeting glutamine metabolism rescues mice from late-stage cerebral malaria. Proc Natl Acad Sci U S A. 2015
46. Martin M. Cutadapt removes adapter sequences from high-throughput sequencing reads. EMBnet Journal. 2011; 17:10–12.
47. Trapnell C, et al. Differential gene and transcript expression analysis of RNA-seq experiments with TopHat and Cufflinks. Nat Protoc. 2012; 7:562–578. [PubMed: 22383036]

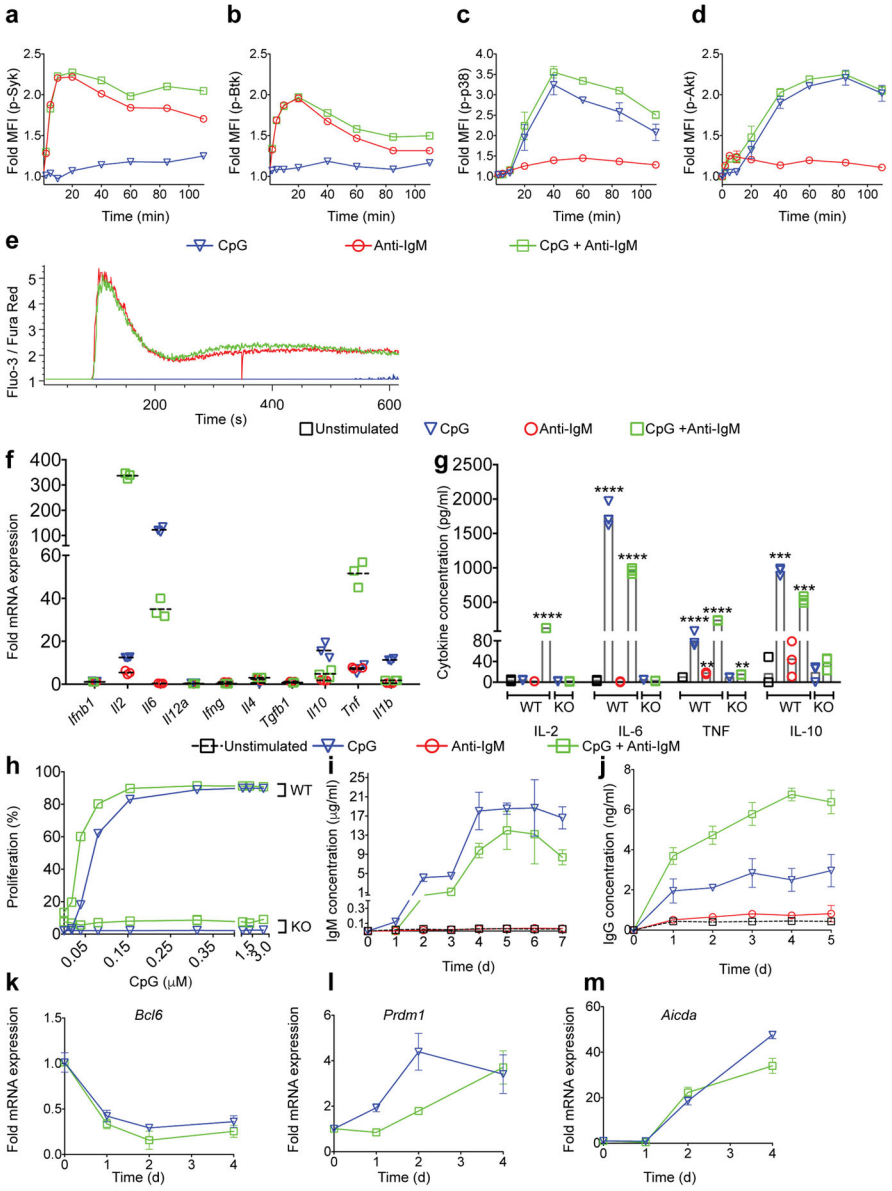

Figure 1. The effect of TLR9 signaling on the outcome of B cell responses to antigen

In all cases purified mouse splenic B cells (WT or TRL9 KO) were stimulated *in vitro* with Anti-IgM (2–5μg/ml) or CpG (1μM) alone or in combination. **(a–d)** Individual B cell samples were fixed and barcoded using combinations of B220-specific antibodies[19], pooled, permeabilized and stained with mAbs specific for the phospho-kinases: p-Syk **(a)**, p-Btk **(b)**, p-p38 **(c)** and p-Akt **(d)**. The fold changes in abundance of phosphorylated kinases in stimulated as compared to unstimulated B cells are shown. **(e)** Calcium flux measured by flow cytometry in B cells loaded with the Ca^{2+} sensor dyes Furo-red and Fluo-4 and stimulated. **(f)** Fold changes in the mRNA expression for various cytokines of B cells stimulated for 4h as compared to unstimulated B cells. **(g)** ELISA measurements of cytokine proteins in the culture supernatants of WT or TLR9 KO B cells stimulated *in vitro* for 18 h (for IL-6) or 24 h (for TNF, IL-2 and IL-10). **(h)** Proliferation of WT or TLR9 KO B cells

stimulated with a sub-optimal concentration of Anti-IgM (1μg/ml) and increasing concentrations of CpG (0 to 3 μM). Shown are the percentage of cells that proliferated after 46 h of culture. **(i,j)** Antibody production by stimulated B cells for a duration of seven days. ELISA measurement of IgM **(i)** and IgG from the IgG^+ deplated B cells (Fig.S1g) **(j). (k–m)** Kinetic analysis of *in vitro* mRNA expression of GC B cell- or PC-specific genes in stimulated WT B cells for 4 days. Expression of *Bcl6* (**k**), *Prdm1* (**l**) and *Aicda* (**m**) is shown as fold changes over that observed in unstimulated B cells at time 0. Data are representative of three independent experiments performed with duplicate (**a–d**), or triplicate samples (**e–n)**. Data points and error bars indicate mean and standard deviation, respectively. Statistical significance was measured using two sided unpaired t-test (**= $0.001<P\leq0.01$; ***=$0.0001<P\leq0.001$; ****=$P\leq0.0001$).

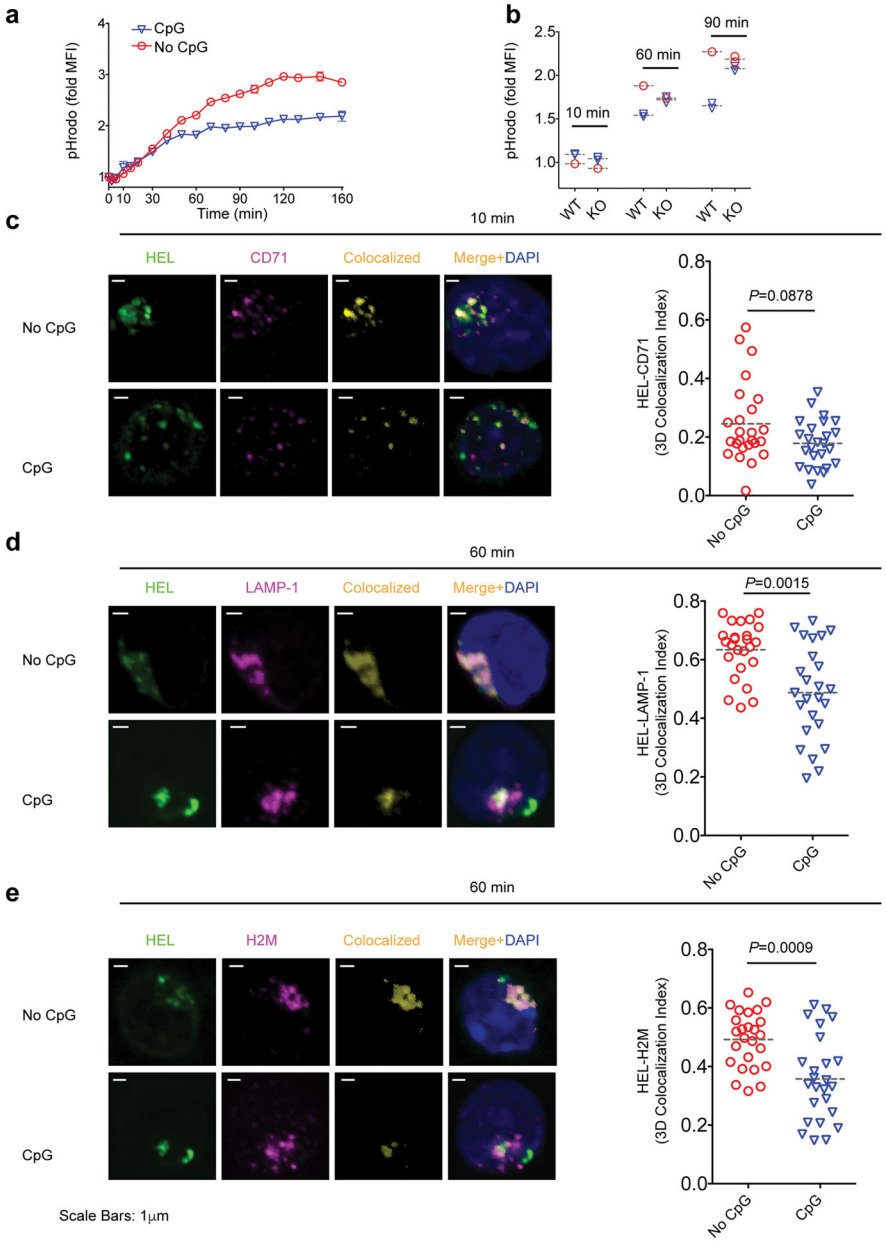

Figure 2. TLR-9 signaling antagonizes the trafficking of BCR-bound antigen into late endosomal compartments

(a) HEL-specific MD4 B cells incubated with pHrodo-conjugated HEL at 37°C in the presence or absence of CpG. The FI of pHrodo was measured over time by flow cytometry. Fold changes in MFI values over the pHrodo MFI prior to incubation are shown. **(b)** Fold changes in pHrodo MFI values for WT MD4 and TLR9-KO MD4 B cells. **(c–e)** MD4 B cells were immobilized on coverslips and incubated with rhodamine-conjugated HEL in the presence or absence of CpG (1μM). Cells were fixed, permeabilized and stained with mAbs specific for CD71, LAMP1 or H2M. Confocal microscopy images of representative cells (left panels) and the 3D colocalization indices of 25 cells per group (right panels) are shown. **(c)** Colocalization of HEL with CD71 at 10 min. **(d)** Colocalization of HEL with LAMP-1 at

60 min **(e)** Colocalization of HEL with H2M at 60 min. Data are representative of three independent experiments. Lines indicate mean values. Lines and error bars represent mean of duplicates and standard deviation of the mean. Statistical significance was measured by two sided Mann-Whitney U test.

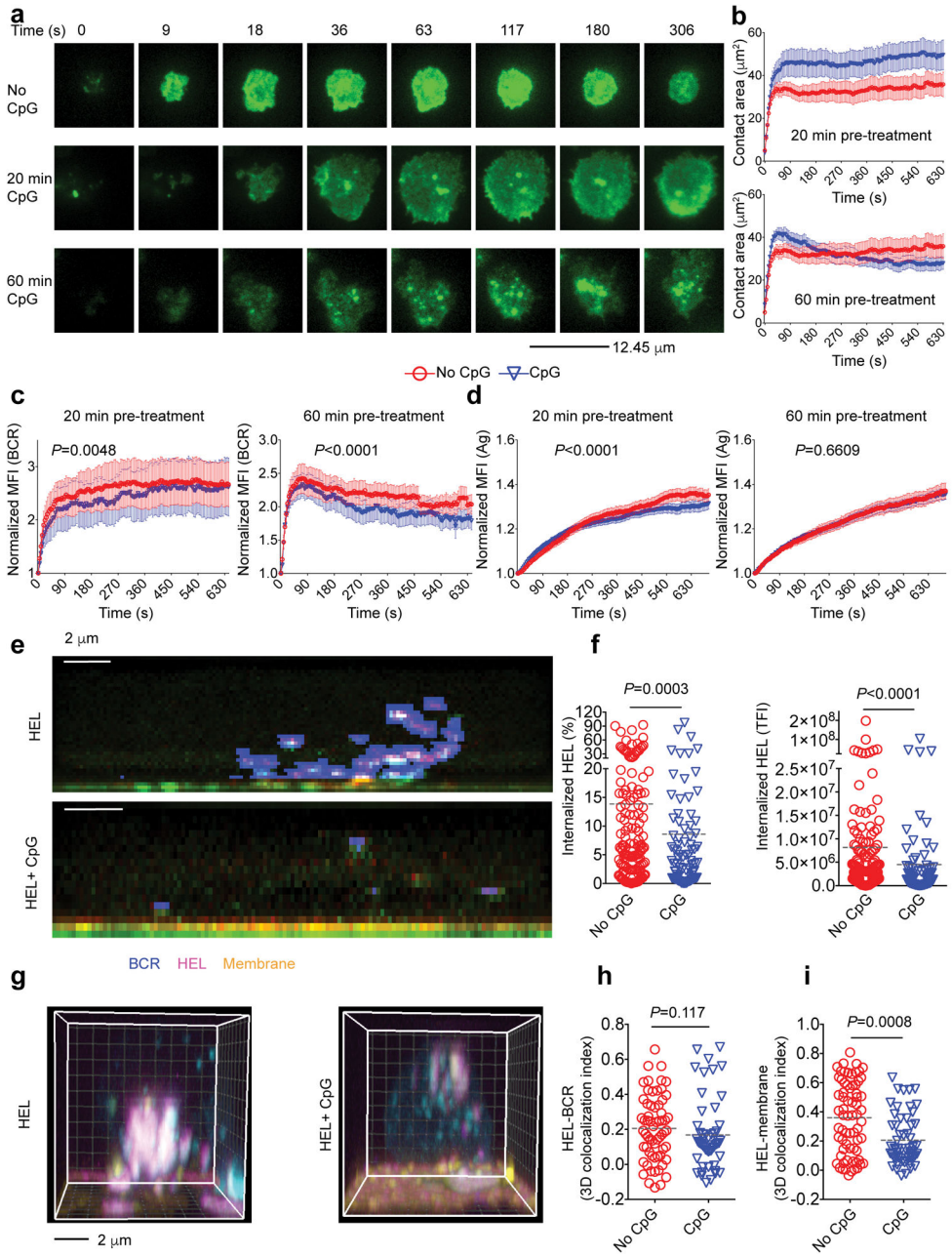

Figure 3. The effect of TLR-9 signaling on B cell responses to membrane bound antigen

(a–d) HEL-specific MD4 B cells untreated or pretreated with CpG (1μM) for 20 or 60 min, labeled with DyLight 649-Fab Anti-IgM and placed on Alexa Fluor 488-HEL-containing PLB. **(a)** Representative time lapse TIRF images of B cell (supplementary Videos, S1a, S1b and S1c). **(b)** Quantification of the contact areas of the B cell with the HEL-containing PLB with time. The accumulation of the BCR **(c)** and HEL**(d)** in the area of contact of the B cell with the PLB. **(e–f)** Untreated or CpG (1μM) treated HEL-specific MD4 B cells labeled with DyLight 649-Fab Anti-IgM and placed on CM-DiI-labeled PMS containing Alexa Fluor 488-HEL for 30 min at 37°C. **(e)** Confocal *z*-stack images reconstituted as an *x* and *z*

sideview using maximal projection along the *y* axis are shown, HEL (magenta), PMS (green) and internalized HEL (cyan). **(f)** The percent of the HEL in the bilayer that was internalized (left); the total internalized HEL taken as the total fluorescence intensity (TFI) (right). **(g)** A 3D-reconstructed image of confocal *z*-stacks showing BCR (cyan), HEL (magenta) and PMS (yellow) (supplementary Videos S2a and S2b). **(h,i)** Quantification of the colocalization of the BCR and HEL **(h)** and HEL and PMS **(i)**. Data represent three independent experiments. Lines indicate mean values. Statistical significance was measured by two sided Quadratic Regression **(c,d)**, two sided Mann-Whitney U test **(f,h,i)**.

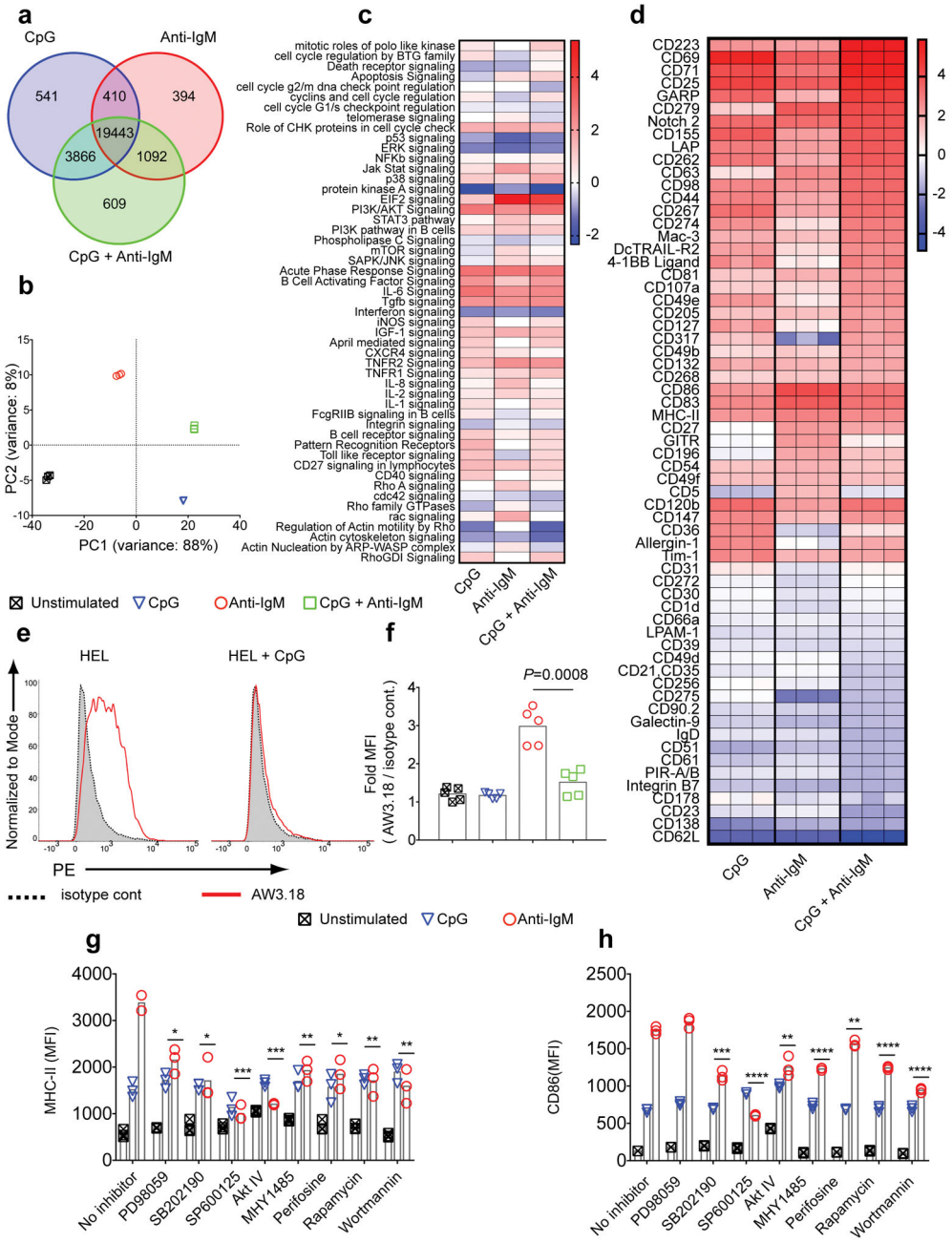

Figure 4. The effect of TLR9 and BCR signaling on B cells transcription and the expression of B cell surface proteins

(a–c) Purified B cells were unstimulated or stimulated with CpG (1 μM) or Anti-IgM (5 μg/ml) or a combination of the two, in triplicate for 4 h *in vitro* and analyzed by RNA seq. **(a)** Venn Diagram and **(b)** principle component analysis showing differentially affected genes. **(c)** Ingeniuty Pathway analysis showing the log2 scale enhanced and diminished transcriptional regulation in various pathways in response to different stimulations relative to unstimulated B cells. Purified B cells were cultured as in **(a)** for 24h, barcoded, and analyzed for the expression of surface proteins using a BioLegend LegendScreen kit. Proteins that

showed an increase of three fold or more or decreased 30% or more as compared to untreated B cells are shown in a log2 scale heat map **(d). (e,f)** HEL-specific MD4 B cells stimulated with HEL (1 μg/ml), CpG (1 μM) or both for 24 h and MHC class II I-A^k-HEL peptide complexes quantified by flow cytometry using the mAb, AW3.18, specific for I-A^k-HEL. Representative flow cytometry plots **(e)** and fold MFI values (MFI of AW3.18 stained cells divided by the MFI of isotype control mAb**) (f)** are shown. **(g,h)** B cells were stimulated with CpG (1 μM) or Anti-IgM (5 μg/ml) in the presence or absence of the following inhibitors: 50 μM PD98059 (MEK 1&2 inhibitor), 10 μM SB202198 (p38 inhibitor), 30 μM SP600125 (JNK inhibitor), 5 μM Akt IV (Akt inhibitor), 10 μM MHY1485 (mTOR activator, autophagy inhibitor), 20 μM Perifosine (Akt inhibitor), 100 nM Rapamycine (mTOR inhibitor), 50 nM Wortmannin (PI3K inhibitor). Surface expression of MHC class II **(g)** and CD86 **(h)** are shown. Values that are significantly decreased compared to no inhibitor condition are shown with asterisks. Data shown in **(d,g,h)** are epresentative of two independent experiment performed in triplicates. Statistical significance was measured using a two sided unpaired t-test (n.s.= $P>0.05$; *=$0.01< P \leq 0.05$; **= $0.001< P \leq 0.01$; ***=$0.0001< P \leq 0.001$; ****= $P \leq 0.0001$).

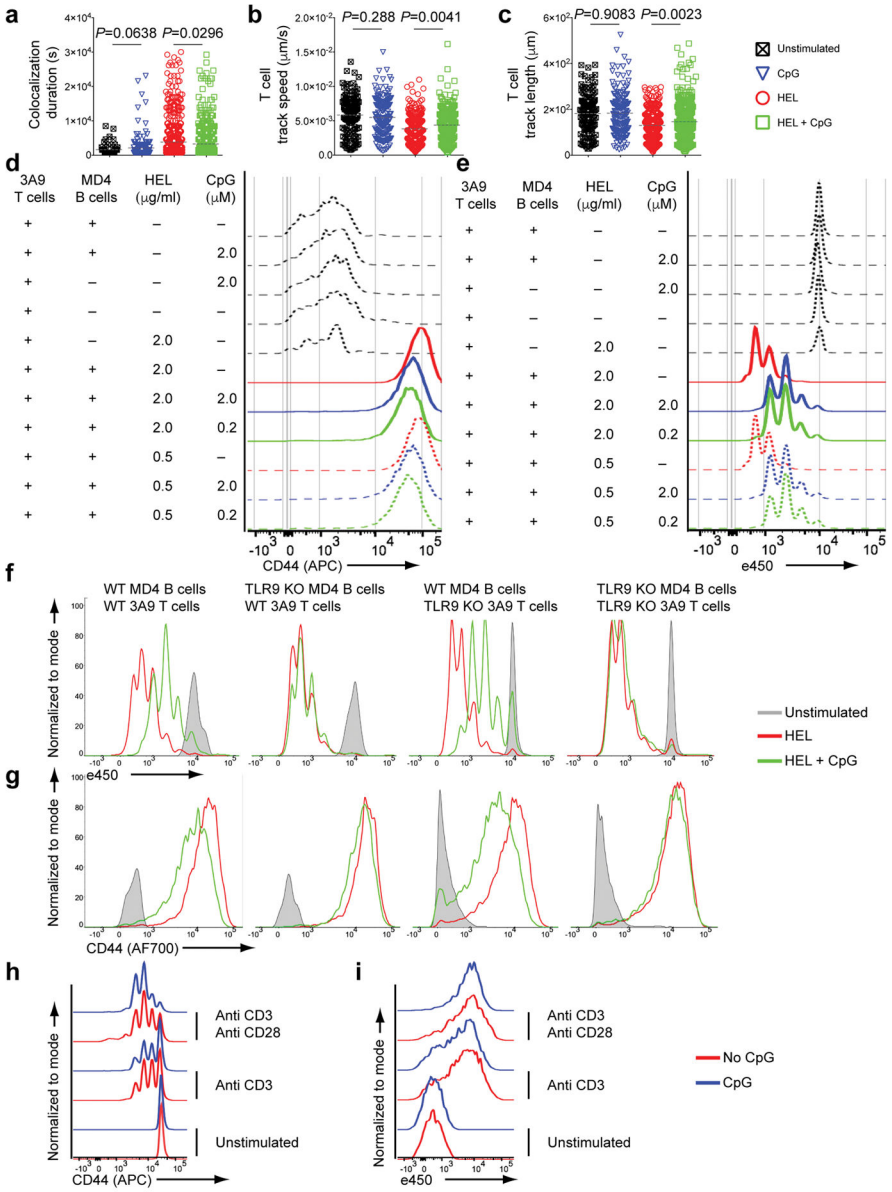

Figure 5. TLR9 signaling decreases the ability of antigen-specific B cells to interact with and activate antigen-specific helper T cells in response to soluble antigen

(a–c) HEL-specific MD4 B cells stained with CMFDA (green) were cultured with 3A9 T cells stained with CMTMR (red) in a 1:1 ratio in the presence or absence of CpG (1μM) and/or HEL (1μg/ml). Interactions of B and T cells were imaged for 24 at rate of 1 frame per 10–20 min. Duration of B and T cell colocalization **(a)**, T cell track speed **(b)** and T cell track length **(c)**. Doted lines indicate the mean values. **(d,e)** CD44 expression **(d)** and profiferation **(e)** of HEL-specific 3A9 T cells stimulated with HEL (0.5 or 2.0 μg/ml), CpG (0.2 or 2.0 μM) and HEL-specific MD4 B cells for 72h. **(f,g)** Proliferation **(f)** and CD44 expression **(g)** of 3A9 $CD4^+$ HEL-specific T cells (WT or TLR9 KO) cultured with HEL-specific MD4 B cells (WT or TLR9 KO) in the presence of HEL (1μg/ml) with or without CpG (1μM) for 72 h. Data represent two independent experiments performed in triplicates.

(h,i) CD44 expression **(h)** and profireration **(i)** of $CD4^+$ T cells stimulated with antibodies specific for either CD3 or CD28 for 72 h in the presence or absence of CpG (1μM). Data are representative of three independent experiments carried out in triplicates. Statistical significance was measured using a two sided Welch's t-test.

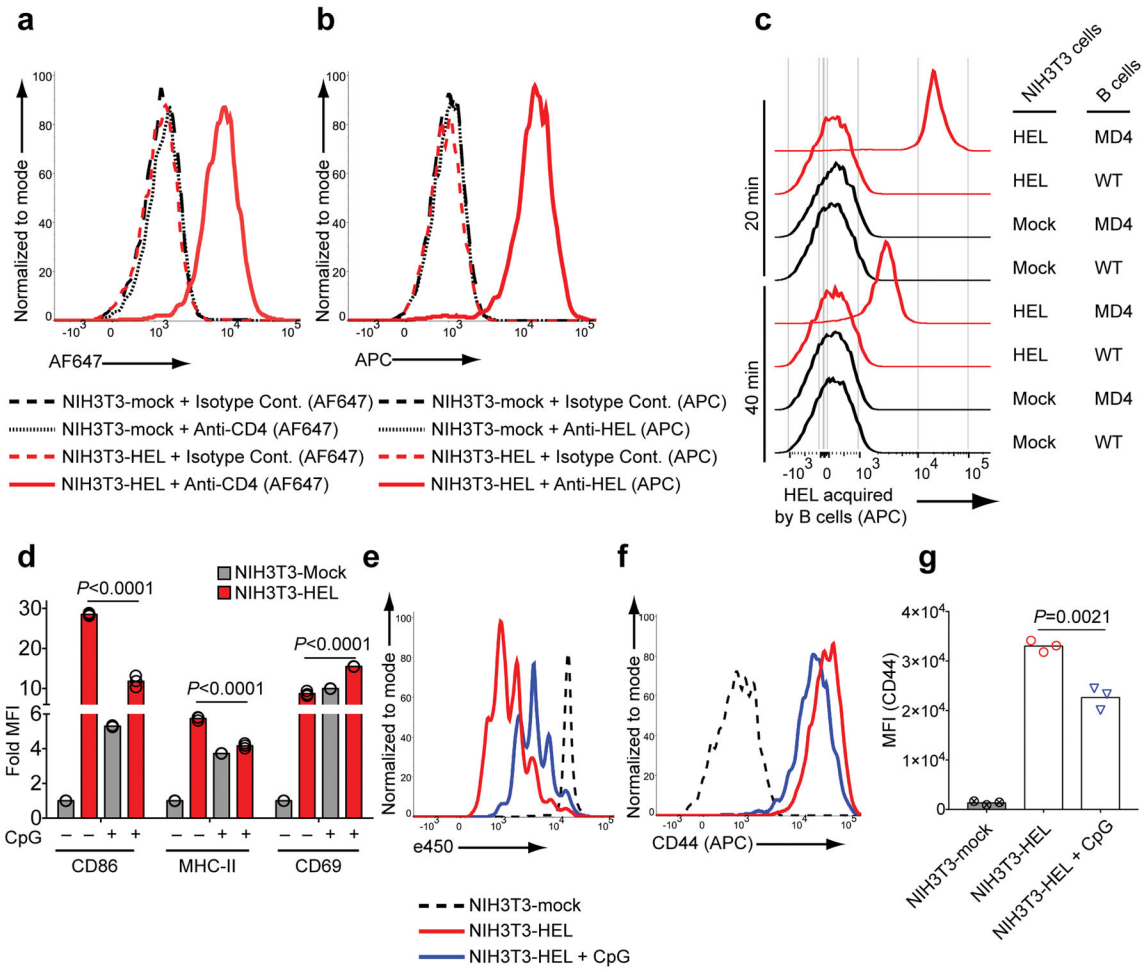

Figure 6. TLR9 signaling decreases the ability of antigen-specific B cells to activate antigen-specific helper T cells in response to membrane bound antigen

NIH3T3 cells were transduced with retroviral vectors containing sequences encoding an HEL-CD4 chimeric membrane protein (NIH3T3-HEL) or a mock vector (NIH3T3-mock). Cell surface expression of the chimeric proteins was quantified using **(a)** a AF647-labeled CD4-specific mAb or **(b)** a APC-labeled HEL-specific mAb. **(c)** Flowcytomerty plots of HEL-specific MD4 B cells or nonspecific B cells incubated with NIH3T3- Mock or NIH3T3-HEL cells for 20 or 40 min, fixed, permeabilized and stained with a HEL-specific mAb. **(d)** Fold changes in the expression of CD86, MHC-II and CD69 for HEL-specific MD4 B cells or nonspecific B cells incubated with NIH3T3-Mock or NIH3T3-HEL cells for 24 h in the presence or absence of CpG (1μM). **(e–g)** T cell proliferation **(e)** and CD44 expression **(f,g)** for HEL-specific 3A9 $CD4^+$ T cells cultured with HEL-specific MD4 B cells and either NIH3T3-Mock or NIH3T3-HEL cells in the presence or absence of CpG (1uM) for 72 h. All data are representatives of three independent experiments performed in triplicates. Bars in graphs indicate means. Statistical significance was measured using two sided unpaired t-tests

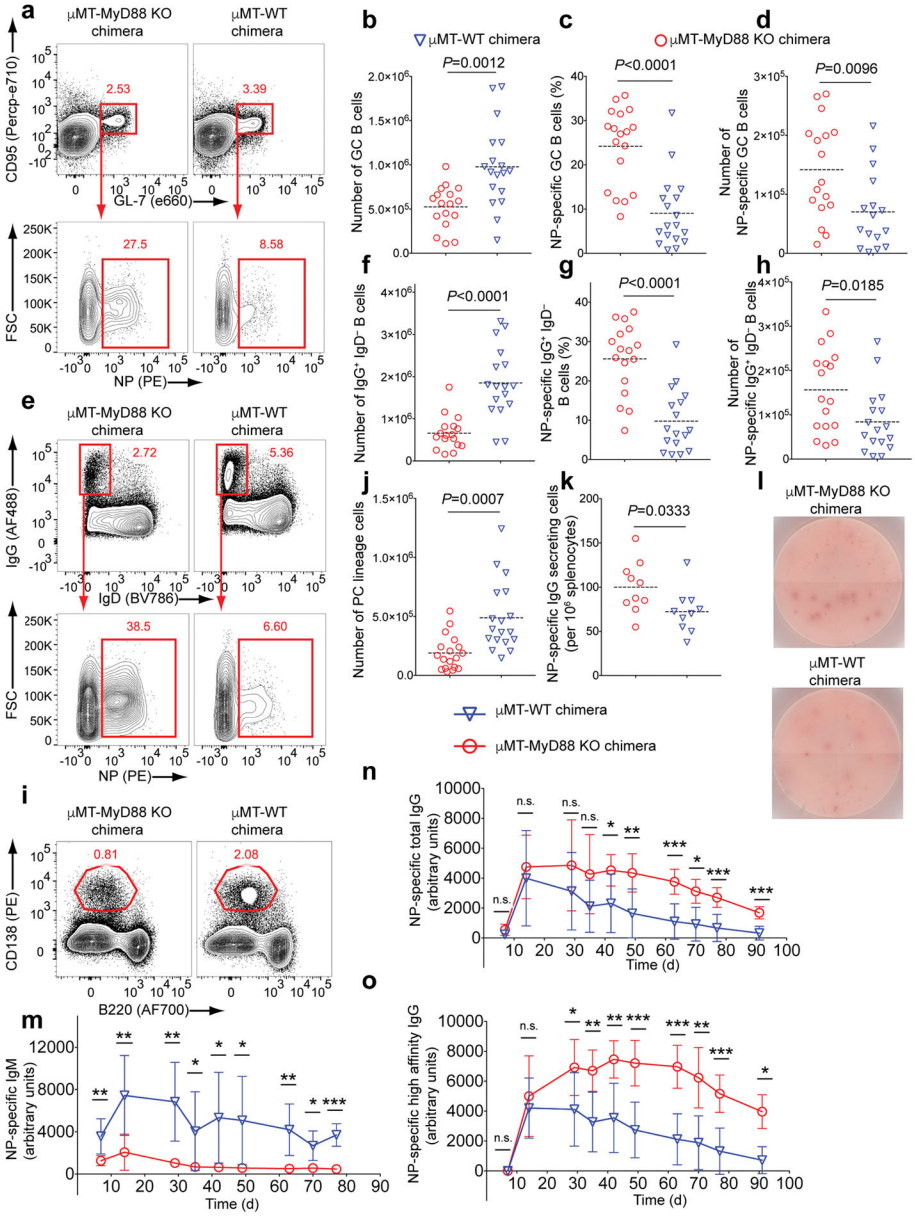

Figure 7. The B cell intrinsic expression of the TLR9 adaptor MyD88 impacts the outcome of T cell dependent Ab response in vivo

Bone marrow chimeras generated as shown (Fig.S5a) were immunized with NP-CGG (100 μg/mouse) adsorbed on Alum (100 μl/mouse) and CpG (65 μg/mouse) and spleens were analyzed on day 14 post immunization. Spleen cells were analyzed by flowcytometry using the gating strategy shown (Fig.S5c). **(a–d)** Representative flow plots **(a),** total number of GC B cells **(b)**, percent of all GC B cells that were NP-specific **(c)** and the total number of NP-specific GC B cells **(d). (e–h)** Representative flow plots **(e)**, total number of IgG^+ IgD^- cells **(f)**, percent of all IgG^+ IgD^- B cells that were NP-specific **(g)** and total number of NP-specific IgG^+ IgD^- B cells **(h). (i–l)** Representative flow plots **(i)** and total number of PC-lineage cells **(j)**. NP-specific IgG Ab secreting cells **(k)** and visualized by ELISPOT **(l).** Data were pooled from two independent experiments. Each symbol represents an individual

mouse. Dotted lines indicate mean values. Statistical significance was calculated using a two sided Welch's t test. **(m–o)** NP-specific IgM **(n)**, NP-specific IgG **(o)** and high affinity NP-specific IgG **(p)** given in arbitrary units calculated from serial dilutions of pooled sera from NP-CGG immunized WT mice. Data represent two independent experiments. Lines and error bars represent the mean of 8 individual mice and SD respectively. A two sided Welch's t test was used to determine the statistical significance. Values that are significantly different between each group for each collection day are shown with asterisks (n.s.= $P>0.05$; *=$0.01< P \leq 0.05$; **= $0.001< P \leq 0.01$; ***=$0.0001< P \leq 0.001$; ****= $P \leq 0.0001$)

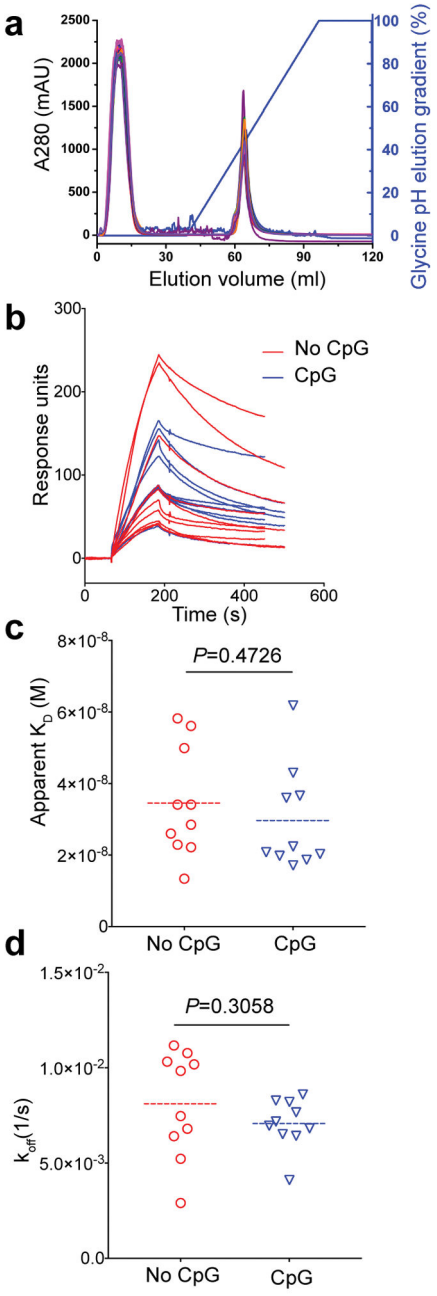

Figure 8. CpG does not induce high affinity antibodies in human

Human subjects were immunized with AMA1-C1, formulated on Alhydrogel with or without 564 μg of CpG 7909. Sera were collected on day 70 post immunization and IgG antibodies were purified using protein G columns. Representative chromatography profiles **(a)** are shown. **(b)** BIAcore binding analysis between PfAMA1 and serum IgGs (70nM). The binding sensorgrams of IgG samples from CpG and Non-CpG immunized subjects are shown in blue and red, respectively. **(c,d)** Apparent K_D binding affinities **(c)** and k_{off} values **(d)** measured by surface plasmon resonance analysis of serially diluted purified antibodies

are graphed. Each symbol represents an individual. Statistical significance was measured using a two sided Welch's t-test